Polymer Chemistry

Accepted Manuscript

This article can be cited before page numbers have been issued, to do this please use: J. Hu, Z. Wang, M. Yang, C. Yu, S. Li, Y. Miao, X. Quan, J. Liu and S. Shao, *Polym. Chem.*, 2024, DOI: 10.1039/D4PY00857J.

ROYAL SOCIETY OF CHEMISTRY

rsc.li/polymers

View Article Online
DOI: 10.1039/D4PY00857J

ARTICLE

Long afterglow epoxidized soybean oil polymer composites with reversible dynamic cross-linking for intelligent coating

Received 00th January 20xx,
Accepted 00th January 20xx

DOI: 10.1039/x0xx00000x

Jiaman Hu,[a] Zihao Wang,[a] Minglin Yang,[a] Chuansong Yu,[a] Siyu Li,[a] Yinggang Miao,[b] Xiangqian Quan,[c] Jize Liu*[a] and Shiyang Shao*[a]

High-performance coatings with advanced functions such as long afterglow luminescence and self-healing have attracted great interest around the world, however, the integration of these desired multifunctions in a single composite system still remains a great challenge. Herein, an intelligent coating based on epoxidized soybean oil and modified long afterglow powders was presented for self-healing intelligent coating. By constructing dynamic hydrogen bonding network between natural polyphenols and epoxidized soybean oil, the obtained composites possess desired adhesive performances and self-healing ability, the shear strength of obtained coating is able to reach 313.96 KPa while the self-healing efficiency was about 81.29% after damage-healing process. Moreover, the introduction of SiO2-modified SrAl2O4: Eu2+, Dy3+ powders endow the intelligent coating with long afterglow ability, which greatly benefit the visualized monitoring of small cracks. Meanwhile, the obtained bio-sourced composites could be degraded under anaerobic composting conditions within 5 days, and after degradation the long afterglow powders could be separated and recycled with almost consistent performances (luminescent intensity maintains 95.19%) contrast to original powders. This study offers valuable examples and new insights for high-value utilization of bio-based materials.

Introduction

Coating on the surface of metal and polymer material is a key method to effectively protect material from corrosion and damaging[1, 2]. When the coating layer is in excellent condition, it offers excellent physical shielding against the corrosive medium, protecting the substrate from corrosion and damage[3-5]. Most existing synthetic coatings are formulated with petrochemical resins, while the weak adhesion to metals and polymer material, inevitable interfacial debonding and micro-crack propagation significantly affect their shielding protection ability, as electrochemical corrosion and microscopic damage development may cause domino-like overall corrosion damage process[6-9]. In addition, petroleum-based coatings, due to their non-biodegradable nature, may lead to further microplastic pollution after being damaged.[10-13]. Therefore, high-performance, advanced-functionality and environmentally-friendly matrices are one of the most important development trends in next-generation coatings, high-adhesion, self-healing and biodegradable smart coatings as a result have attracted extensive attention from researchers worldwide[14, 15].

Bio-based and bio-degradable materials are gradually becoming another new leading industry that drives scientific and technological innovation and economic development in the contemporary world due to their green, environmentally friendly, and low-carbon characteristics[16, 17]. Through elaborate multi-scale structure design to endow the bio-based materials with desired comprehensive performance which can match or even exceed that of petroleum-based coatings is a highly attractive topic, but it remains a formidable challenge[15, 18, 19]. For example, Yang et al. isolated water-insoluble lignin from biomass and obtained a simple bio-based wood adhesive. Through the self-cross-linking of lignin during the hot-pressing process, high-performance wood adhesive was achieved after 100 °C for 2 min, and the adhesive strength could reach the Chinese National Standard GB/T 9846-2015[20]. Sun et al. prepared a novel bio-based supramolecular adhesive based on castor oil, melevodopa and Fe^{3+} ions. Owing to the strong coordination interaction between melevodopa functionalized castor oil and Fe^{3+} ion, as well as the catechol units of melevodopa, the obtained adhesives achieved adhesion strengths of 14.6 MPa at room temperature and 9.5 MPa at -

[a] School of Materials Science and Engineering, Hainan University (Haikou, 570228, Hainan, China)
[b] Shaanxi Key Laboratory of Impact Dynamics and its Engineering Application, School of Aeronautics, Northwestern Polytechnical University, Xi'an 710072, China; Joint International Research Laboratory of Impact Dynamics and its Engineering Applications, School of Aeronautics, Northwestern Polytechnical University, Xi'an 710072, China; National Key Laboratory of Strength and Structural Integrity, Xi'an 710072, China
[c] Institute of Deep-Sea Science and Engineering, Chinese Academy of Sciences, Sanya 572000, China; Department of Mechanical and Aerospace Engineering and Scripps Institution of Oceanography, University of California San Diego La Jolla, CA 92093, USA
*Corresponding authors: Jize Liu (E-mail address: ljz@hainanu.edu.cn) and Shiyang Shao (E-mail address: ssyang@hainanu.edu.cn)
†Long afterglow epoxidized soybean oil polymer composites with reversible dynamic cross-linking for intelligent coating.
Supplementary Information available: [details of any supplementary information available should be included here]. See DOI: 10.1039/x0xx00000x

196 °C, it is the highest value reported for bio-based adhesives and supramolecular adhesives[21]. Among the widely used bio-sourced polymer materials, epoxy soybean oil is an ideal candidate for the development of commercially viable environmentally friendly bio-based coatings because of their inexpensive and readily available characteristics[22, 23]. However, the low cohesion energy and weak reactivity of non-polar epoxy soybean oil always led to unsatisfactory adhesion and mechanical properties. Till now, how to design environmentally friendly cross-linking systems for high-performance epoxy soybean oil-based coating applications is still a crucial research direction[24, 25].

Optical signals account for 70% of the information received by humans, the construction of luminous behaviour as a result offers new opportunities for intelligent applications of organic coatings[26]. Long afterglow materials, which are able to store the acquired light energy and release it in the form of light continuously and slowly after removing the external light source, have attracted increasing attention for advanced applications in emergency lighting, traffic signs, interior decoration, display, anti-forgery and other fields[27-29]. For example, Liu et al. designed a novel near-infrared-persistent luminescence material $(Sr,Ba)(Ga,In)_{12}O_{19}:Cr^{3+}$ with efficient ultraviolet (UV)-red light charging capacity. After being mixed with acrylic acid the obtained afterglow coating could be applied to metal for infrared tagging, which the image can last for more than one day at night[30]. Zhou et al. prepared hour-scale ultra-long afterglow polymer films by molecular doping strategy. The afterglow of transparent and flexible polymer films can last for 11 h in air at room temperature and can be used for efficient flexible display including information writing and erasure[31]. As a typical afterglow material, $SrAl_2O_4$: Eu^{2+}, Dy^{3+} possesses advantages including long and strong visible afterglow, which is able to endow the composite coatings with battery-free illumination during night and is expected to increase the added value of coatings[28]. However, the widely used $SrAl_2O_4$: Eu^{2+}, Dy^{3+} powder undergo hydrolysis when contact with water, which may lead to a serious degradation of polymer matrix and limit their application[32].

As mentioned above, the propagation of micro-cracks and the infiltration of small molecules (like water, oxygen, and ions) can accelerate metal corrosion through the electrochemical process, so early warning and spontaneous repair of micro-cracks are of crucial significance[33-35]. By introducing modified long afterglow $SrAl_2O_4$: Eu^{2+}, Dy^{3+} powder, the luminescence intensity and distribution of obtained coatings will change under stress and defect conditions, which is expected to be applied to the non-contact and dynamically visualized monitoring of stress concentration and small cracks, and warning technique can be achieved through the development of new analysis and identification technology[36-38]. In addition, the multiple hydrogen bonds design endows the coating with self-healing ability to repair small cracks, which could be able to significantly delay the corrosion process of metals and damage problems of polymer material, providing a feasible strategy for the realization of green and long-life intelligent coatings[39].

Herein, this paper presents an environmentally friendly, recyclable, long afterglow smart coating using natural bio-based materials and long afterglow materials for self-healing intelligent coatings. Epoxidized soybean oil (Soy) was cured by malic acid (Mal) and tannic acid (Ta) at first, the obtained Soy-Mal-Ta (SMT) bio-sourced polymer with a large number of hydrogen bonds and polyphenol hydroxyl groups for the metal-polyphenol network (MPN) endows the coating with strong adhesion, and ability to repair small cracks after damage. By incorporating $SrAl_2O_4$: Eu^{2+}, Dy^{3+} powder modified with silane coupling agent containing epoxy groups, the long afterglow powders were composited with the bio-sourced matrix through strong covalent-noncovalent interfacial cross-linking, which greatly benefit the achievement of visualized warning system for capturing the crack situation. Furthermore, the bio-sourced matrix could be bio-degraded in the soil while the modified powders could be reused through a simple density sorting process, which better conforms to the trend of a low-carbon future. This strategy is designed to meet the demand for advanced functional coatings with high adhesion, flexibility and damage warning functions for steel cracking prevention, which offers important examples and ideas for high-value utilization of bio-based materials.

Experimental

Materials

Tannic acid (>96.0%) was purchased from Jiangsu Aikang Biomedical R&D Co., Ltd. (China). Malic acid (98.0%) was purchased from Shanghai Boka Chemical Technology Co., Ltd. (China). Epoxy soybean oil (ESO, 95.0%) was purchased from Guangzhou Suixin Chemical Co., Ltd. (China). $SrAl_2O_4$: Eu^{2+}, Dy^{3+} powder was purchased from Chuangrong Chemical Technology Co., Ltd. (China). Anhydrous ethanol (AR, >99.7%) was purchased from Shanghai Titan Technology Co., Ltd. (China). Hydrochloric acid (HCl, AR), Sodium chloride (NaCl, AR, >99.5%) was purchased from Xilong Science Co., Ltd. (China). 3-(Glycidoxypropyl)triethoxysilane (GC, >96.0%) was purchased from Shanghai Aladdin Biochemical Technology Co., Ltd. (China). Urea (AR, 99.0%), Tetraethyl orthosilicate (TEOS, GC, 99.0%) and ammonium bicarbonate (AR) were purchased from Shanghai Yien Chemical Technology Co., Ltd. (China). All the reagents were used as received without further purification. The water used in all experiments was deionized and ultrafiltered to 18.2 MΩ•cm with an Ulupure ultrapure water system (China).

Preparation of modified $SrAl_2O_4$: Eu^{2+}, Dy^{3+} powder

Firstly, 0.40 ml TEOS was dissolved in a 200 ml mixture of distilled water and ethanol (volume ratio of 1:1). Then a suitable amount of hydrochloric acid was added to adjust the pH value to 1, and placed under this condition for 30 min until the solution was clarified and transparent. Afterwards, ammonium bicarbonate was added to set the pH value to 6. After stirring for 5 min and increasing the temperature to 65 °C, 15 g urea and 15 g $SrAl_2O_4$: Eu^{2+}, Dy^{3+} powder was added into the solution, the continuous addition of urea brought the PH to about 10 and

View Article Online
DOI: 10.1039/D4PY00971

kept under stirring for 2 h. After that, the suspension was kept at room temperature for 1 h, then the powder was separated by filtration and washed with deionized water. Finally, the obtained SiO_2-modified powder was dried in an oven at 90 °C for 2 h. A mixture of dried modified SiO_2 powder and 3-(Glycidoxypropyl)triethoxysilane solution (volume ratio 1:0.2) was added to 100 ml of distilled water. After stirring for 10 min and increasing the temperature to 65 °C, keep under stirring for 2 h. Then the powder was separated by filtration and washed with deionized water. Finally, the powder was dried in an oven at 90 °C for 2 h.

Preparation of modified $SrAl_2O_4$: Eu^{2+}, Dy^{3+} SMT coatings

One gram of epoxy soybean oil was added to a round-bottomed flask and heated to 70 °C in an oil bath. After sufficiently heating to decrease viscosity, 1 ml of a 0.5 g/ml tannic acid/ethyl alcohol solution was added to the epoxy soybean oil and mixed for about 5 min. Next, 0.4 g of malic acid was slowly added to the solution until completely dissolved. Heat the reactants overnight, remove from the oil bath and cool to room temperature. The reactant was poured into a disposable petri dish, the modified $SrAl_2O_4$: Eu^{2+}, Dy^{3+} was added, and the SMT coating was obtained by mixing it evenly with glass rods.

Lap shear tests

Lap shear tests were conducted on SMT coating-adhered substrates using the WDW-1 microcomputer-controlled electronic universal testing machine from Jinan East Testing Machine Co., Ltd, China, with a testing speed of 500mm/min and a substrate overlap area of 12.0×20.0 mm^2. Lap shear strength (or adhesive strength) is defined as the maximum debonding force obtained through lap shear tests divided by the overlapping area of adhesive.

Electrochemical impedance spectroscopy (EIS) tests

The anticorrosion performance of the SMT coating coated steel was studied in 3.0 wt.% NaCl solution through EIS analysis using an electrochemical station (CHI660E, Shanghai Chenhua). The frequency ranges were 10^5 to 10^{-1} Hz. The EIS measurements were performed on 3 cm^2 of carbon steel samples coated by pure steel and SMT coatings in a three electrodes cell including saturated calomel electrode (SCE) as reference electrode, platinum rod as counter electrode, and coating/steel sample as working electrode.

SMT coating degradation and $SrAl_2O_4$: Eu^{2+}, Dy^{3+} powder recycle test

Paint degradation experiments were performed at room temperature. The above coating (2 g) was buried under the wet bamboo powder for about 2 cm. The degradation of the coating was observed by removing the bamboo powder every other day, and the degraded coating was irradiated with a UV torch (365 nm, 8 w), and the images were captured and saved by a camera. After the coating was completely degraded, the mixture of powder and bamboo powder was removed and added to 250 ml of deionized water, followed by the addition of an appropriate amount of cellulase. After continuous stirring for 5 min, the temperature was increased to 65 °C and continued stirring for 3 to 5 h. The powder is filtered, separated and then dried in an oven at 80°C.

SMT coatings self-healing process

The process of crack self-healing was observed with an electron optical microscopy (Lingling Star 4800-B Guangzhou Xinfun Technology Co., LTD). The coating was evenly coated on the iron sheet, scratches were generated on the surface of the coating using a surgical blade (to simulate the generation of cracks), and the SMT coating was placed under an electron microscope, images were captured by a CCD camera, and video was recorded.

Ultraviolet (UV) resistance test of SMT coatings

Ultraviolet (UV) dark box (length, width and height: 265, 185, 95 mm) made of an iron box and a UV lamp (6 W), the sample is placed in the middle of the box, a UV lamp is placed (5cm) directly above it, the effective irradiation area is 117.75 $x10^{-4}$ m^2, then the irradiation intensity of UV lamp is 509.55 W/m^2. The cumulative exposure time, respectively for 36 h, 72 h, 108 h, 144 h, 180 h, respectively for the UV-36 h, UV-72 h, UV-108 h, UV-144 h, and UV-180 h SMT coating. By measuring the surface temperature of the sample (28 ℃) (Figure S1), the temperature increased only slightly.

Scanning electron microscopy (SEM)

The microscopic morphology of the experimental samples was observed by JSM-6710F SEM (Hitachi, Japan) at an accelerating voltage of 10 kV, prior to SEM observation, the samples were sprayed with gold (10 mA,50 s).

Fourier transform infrared (FTIR) spectroscopy

The FTIR analysis was recorded through an FTIR spectrometer (model Frontier Dual Ranger, PerkinElmer, Waltham, MA, USA) in attenuated total reflectance (ATR) mode from 400 to 4000 cm^{-1} at room temperature, at 4 cm^{-1} resolutions and 32 scans. FTIR data was then normalized and analysed using OriginPro 2021.

Laser confocal microscopy Raman spectroscopy

Laser confocal microscopy Raman spectroscopy (HORIBA, HR Evolution, France) with a 532 nm laser line was performed to characterize the spatial distribution of the different components.

Afterglow attenuation test

The time-resolved contour photoluminescence (PL) maps of SMT coatings collected on FLS-1000. spectrofluorometer (Britain, Edinburgh Instrument) equipped with an Xe lamp as the excitation source, the excitation time is 1200 s, and the collection time is 5800 s.

Results and discussion

Design Principle and Preparation

Most of the existing coatings are based on petroleum-based chemical engineering products, the inevitably occurring cracks during service life may lead to serious metal corrosion and microplastic pollution. It is of great significance to develop green, bio-sourced, and bio-degradable coatings with advanced functions like self-healing and crack monitoring. However, the tiny crack repair and visualized monitoring still remain a challenge. In this study, bio-based materials enrich in multiple reversible hydrogen bonds combined with long afterglow materials were designed for intelligent coating. As shown in

View Article Online
DOI: 10.1039/D4PY00857J

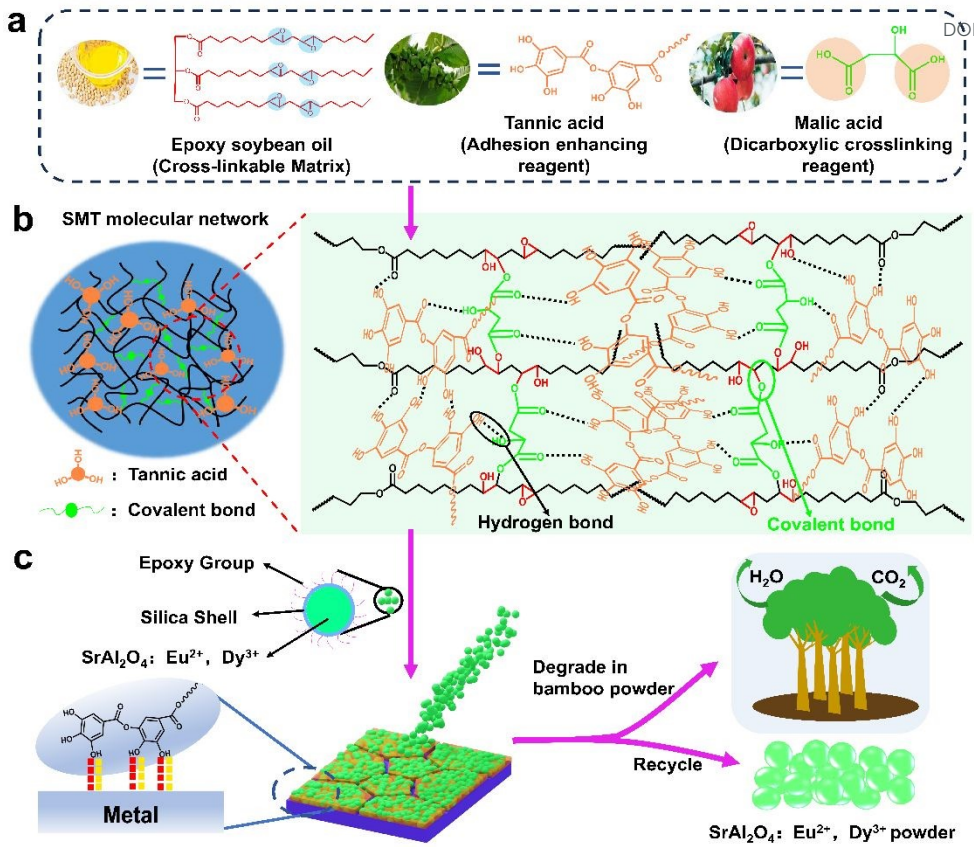

Figure 1. (a) Soy-Mal-Ta (SMT) product are obtained by the reaction of bio-sourced epoxy soybean oil (Soy), tannic acid (Ta), and malic acid (Mal), as well as the molecular structure formulas of the reactants. (b) Molecular network of Soy binding to Mal and Ta in SMT products, rich non-covalent interactions involving hydrogen bonds and phenolic hydroxyl groups. (c) The modified $SrAl_2O_4$: Eu^{2+}, Dy^{3+} powders are simply mixed into the SMT product, the SMT coating is applied to the substrate, where the interaction of the metal matrix with the polyphenol, and the coating is degraded and recycle powder.

Figure 1, a bio-sourced intelligent coating was designed, made from epoxidized soybean oil, malic acid, and tannic acid (Figure. 1a), the epoxidized soybean oil (Soy) was cured by malic acid (Mal), and tannic acid (Ta), the obtained Soy-Mal-Ta (SMT) bio-sourced polymer with a dynamic cross-linked network (Figure. 1b). The cross-linking network involved covalent bonding (epoxy-ring opening reaction with the carboxyl group of malic acid) and noncovalent bonding (hydrogen bondings between phenolic hydroxyl groups of Ta and carboxyl groups of malic acid), such covalent-noncovalent crosslinking network, could significantly benefit the mechanical properties and is expected to endow the materials with recycled, reprocessed, and self-healing ability[40, 41]. Moreover, long afterglow $SrAl_2O_4$: Eu^{2+}, Dy^{3+} powders modified to increase the powder compatibility in functional coatings. By utilizing the luminescent properties of $SrAl_2O_4$: Eu^{2+}, Dy^{3+} powders, can enable to a crack visualization and early warning system. At the same time, the system is rich in a variety of reversible hydrogen bonds and coordinate interaction between tannic acid and metal substrate (Figure. 1c), so that the crack could be able to heal in a short time[42, 43]. Obviously, this study uses natural bio-sourced materials as raw materials, which is in line with the concept of sustainable development and environmental protection. At the same time, these materials are biodegradable, and the $SrAl_2O_4$: Eu^{2+}, Dy^{3+} powder can be recycled after the degradation of the coating (Figure. 1c). The design of high-performance, multi-functional composite long afterglow coatings with reversible dynamic cross-linked networks can provide valuable advice for early warning of coating cracks and for sustainable materials.

Characterization of SMT coating structure and mechanical properties

According to reported literatures, $SrAl_2O_4$: Eu^{2+}, Dy^{3+} powders undergo hydrolysis when in contact with water, and the pH value increases significantly, which greatly limits their application in functional coatings[44]. As shown in Figure 2a, in order to prepare SMT composite coatings, the SiO_2 protective layer was successfully constructed and epoxy groups were grafted on the surface of the protective layer to prevent the hydrolysis of $SrAl_2O_4$: Eu^{2+}, Dy^{3+}, and facilitating better compatibility with SMT coating. In Figure 2b, compared with unprocessed $SrAl_2O_4$: Eu^{2+}, Dy^{3+} powder, the silica-modified $SrAl_2O_4$: Eu^{2+}, Dy^{3+} powder exhibits an obvious peak at around 1098 cm^{-1}, which is ascribed to the Si–O bonding. At the same time, there is a clear peak near 958 cm^{-1}, which is attributed to the epoxy group in the modified $SrAl_2O_4$: Eu^{2+}, Dy^{3+} powder. These results indicate that the SiO_2 layer has been successfully constructed. Due to the presence of the silica layer, the obtained powder can be dispersed in water without hydrolysis, and the pH of the modified powder suspension is about 7, while the pH of the unmodified $SrAl_2O_4$: Eu^{2+}, Dy^{3+} powder suspension

View Article Online
DOI: 10.1039/D4PY00877J

is almost 8-9 after being dispersed in water for 1 h (Figure S2). In order to explore the influence of the SiO_2 protective layer on the PL intensity of the powder, through comparative analysis, it is shown that the $SrAl_2O_4$: Eu^{2+}, Dy^{3+} powder with the SiO_2 protective layer exhibits a higher attenuation degree than the unmodified powder after the excitation source is removed (Figure S3).

The chemical structure of SMT coatings was analysed by Fourier Transform infrared spectroscopy (FTIR). In Figure 2d, for the epoxy soybean oil, a peak at 950 cm^{-1} can be observed that correlates with the presence of epoxy groups[45]. In the FTIR spectrum of the product, termed SMT, the stretching vibration peak of ester group -C=O and C-O-C were observed at 1738 cm^{-1} and 1090 cm^{-1} respectively. The characteristic peak at 3165 cm^{-1} is attributed to hydrogen bond interaction between the phenolic hydroxyl group and the carboxylic acid group[46, 47]. Furthermore, the intensity of C=O characteristic peak of Malic acid decreases and the characteristic peak at O-H disappears. These changes can be attributed to the reaction between the epoxy group in Soy and −COOH in Malic acid[22, 48]. The reaction temperature between the phenolic hydroxyl group of tannic acid and the epoxy group was above 200 °C under the catalyst condition[49]. In this study, it reacted slowly but also participated in the cross-linking reaction of the whole system. SMT is an extensively cross-linked matrix and all three components are involved in covalent bond formation and the system is characterized by a large number of hydrogen bonding interactions[50].

As shown in Figure 2e, the SEM image can be observed in white for the modified $SrAl_2O_4$: Eu^{2+}, Dy^{3+} powder with an average particle size of 0.5 μm. When cracks occur under stress, and the luminance at the crack area differs from other regions, it may be used for early warning. In Figure 2f, laser confocal Raman microspectroscopy with a near-infrared (532 nm) laser and 3D Raman mapping was used to demonstrate the spatial distribution of the different components. Peaks around 2514 cm^{-1} (yellow shadow region) belong to the characteristic region of modified $SrAl_2O_4$: Eu^{2+}, Dy^{3+} powders (Figure S4), and the green to blue areas reveal the spatial distribution of the selected powders. The powder has been successfully loaded into the SMT polymer to form SMT composited coating.

In order to evaluate the applicability and bond strength between the coating and substrate of SMT coatings, lap shear tests were performed on bonded sheets made of different materials using SMT coatings. In Figure 3a, it can achieve bonding functions for different materials (such as glass, PP, PVC, PS, and PTFE). Figure 3b illustrates a shear experiment in which the material is subjected to forces parallel to the coating. As shown in Figure 3c, d, SMT coatings can be tightly bonded to various materials, and the bonding strength of PTFE, Fe, PET, PI, PVC, and PC is 99.33, 164.70, 219.30, 221.83, 297.46, and 313.96 KPa, respectively. SMT coating is able to not only achieve adhesion to metal but also have ideal adhesion ability to polymer materials. The wide applicability of SMT coatings is due to the fact that catechol units can interact with different materials through hydrogen bonding, metal-ligand coordination, hydrophobic effects, etc[51]. As shown in Figure 3e, f, the shear test was carried out using PC material at different tensile speeds. When the tensile speeds were 500, 100, 50, 10, 1, and 0.1 mm/min, the shear strength of PC was 313.96, 110.33, 40.62, 25.45, 9.18, and 1.18 KPa, respectively. It can be concluded that as the tensile speed increases, the bond strength becomes larger, and the PC material exhibits strain rate dependence. As shown in Figure. 3g, the shear toughness at different tensile velocities is obtained by further calculating the stress-strain curves of the shear strength in Figure. 3e. The shear toughness for the tensile speeds of 500, 100, 50, 10, 1, and 0.1 mm/min were 3.1081, 1.1006, 0.6043, 0.1477, 0.0537,

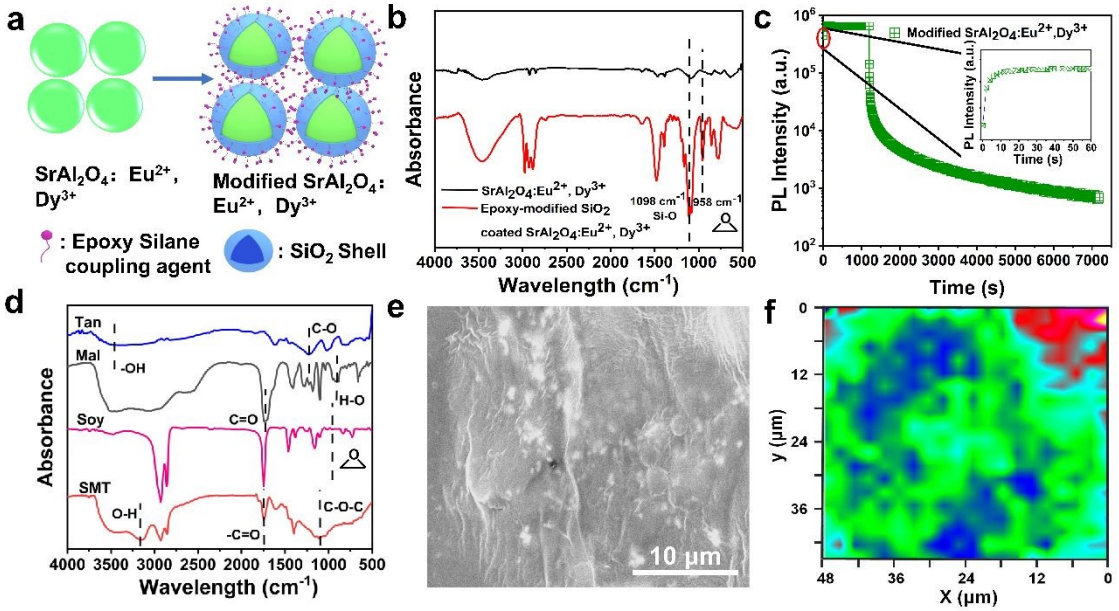

Figure 2. (a) Schematic diagram of $SrAl_2O_4$: Eu^{2+}, Dy^{3+} powder modification. (b) Comparison of FTIR spectra before and after $SrAl_2O_4$: Eu^{2+}, Dy^{3+} powder modification. (c) Afterglow attenuation curve of the modified $SrAl_2O_4$: Eu^{2+}, Dy^{3+} powder. (d) FTIR spectra of Tan, Mal, Soy, and the SMT product. (e) The SEM images of fracture surfaces for the SMT coating. (f) 2D Raman intensity mapping of the obtained SMT coating.

View Article Online
DOI: 10.1039/D4PY00857J

and 0.0197 MJ/m3, respectively. The results show that the shear toughness of SMT coatings increases with the increase of tensile speed. To verify the effect of crosslinking density on SMT coatings, different amounts of tannic acid (which provide hydrogen bonds interactions primarily) were utilized. As shown in Figure S5, with the increase of tannic acid the mechanical properties increase at first and then decrease, the highest shear strength was observed in the samples with a tannic acid content of 0.5 g. The effect of strain rate strengthening exhibited by coatings is more beneficial for materials to withstand high-speed loading conditions such as impacts, improving the protective properties of the metal substrate material. Excellent self-healing ability is massively important for actual applications

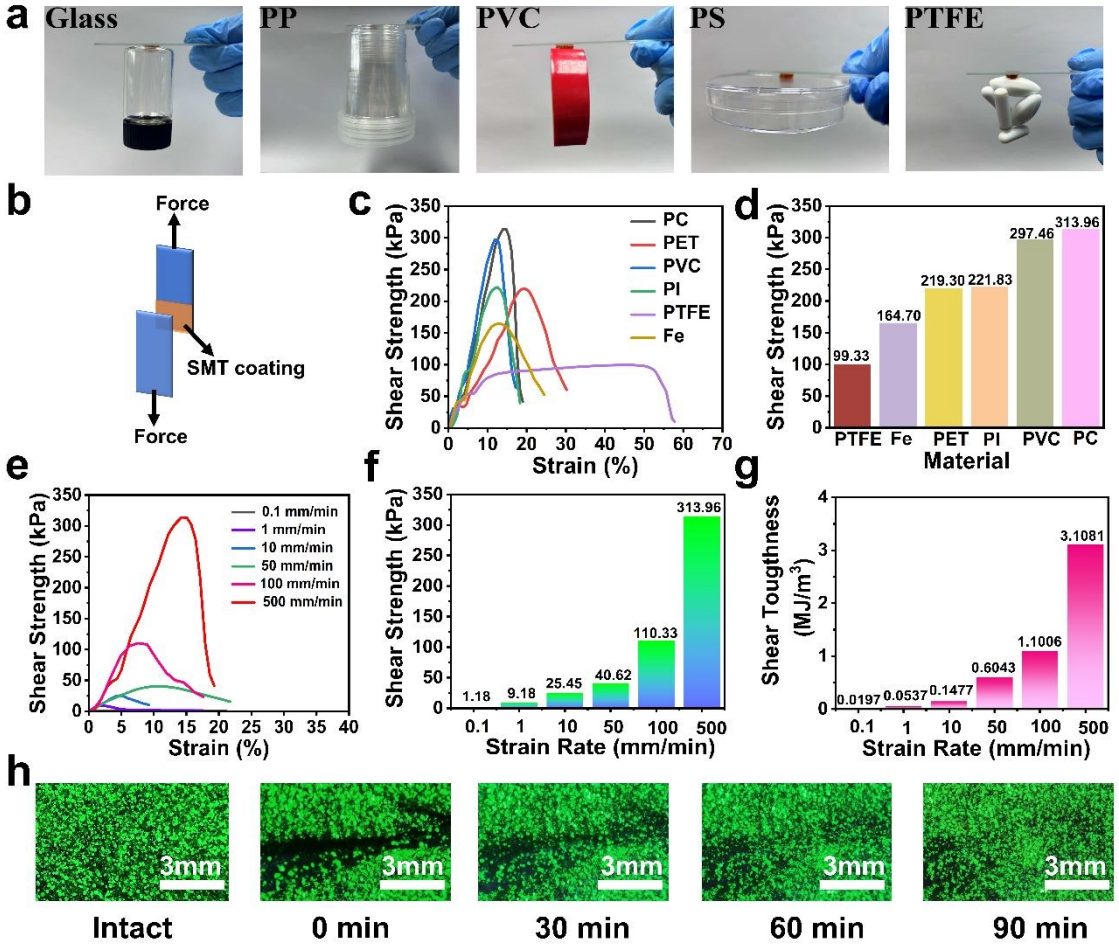

Figure 3. Mechanical properties of SMT coatings. (a) SMT coatings adhering to different materials. (b) Schematic diagram of SMT coatings in shear experiments. (c) Stress-strain curves of SMT coatings in shear strength of different materials. (d) Shear strength of SMT coatings under different materials. (e) Stress-strain curve of the shear strength of SMT coating bonded to PC material at different strain rate. (f) The maximum shear strength of PC at different strain rate. (g) The fracture energy of PC at different strain rate. (h) The self-healing process of the surface crack of SMT coating at 35 ℃.

of coating. To verify the self-healing ability of our SMT coating, the surface of the sample was scratched with a surgical blade, and the samples were self-healed at 35 ℃. Since SMT coating is non-transparent, continuous observation with an electron optical microscopy showed that samples with scratches can recover to its original state under 35 ℃ and the scar at the damage site almost completely disappeared, the whole process lasted for 90 min (Figure 3h, Movie S1). The healed coating was subjected to a lap shear test. The lap shear test results show the excellent self-healing performance of the SMT coating, which possesses a relatively high shear strength of 255.23 KPa after healing process (Figure S6), and the shear strength was maintained above 81.29% after self-healing. The Self-healing ability of SMT coating is through the polyphenols-metal coordination bond, a large number of hydrogen bonds and so on the reversible dynamic non-covalent bonds restructuring to restore the damaged structure and state[42, 43, 52]. The achievement of self-healing also relies on the segmental motion of macromolecules which provides possibilities for the sufficient dissociation and reconstruction of H-bonds. Differential scanning calorimetry (DSC) was carried out (Figure S7) and the glass transition temperature (T_g) of SMT coating is -1.1 °C, which indicate that under room temperature the chain segments possess desired motion ability to support the self-healing behaviors.

Application of Photoluminescence (PL) behaviour in crack detection and analysis

The luminescence performance of SMT coating was investigated. Figure 4a shows the PL intensity and afterglow attenuation behaviour, the $SrAl_2O_4$: Eu^{2+}, Dy^{3+} powder and SMT coating were evenly mixed and excited by the Xe lamp for 20

View Article Online
DOI: 10.1039/D4PY00571

min. The overall afterglow decay behaviours along with time show a quick downward trend within 60 min and then levels off till 90 min. Figure 4b shows the afterglow decay curve after 36 h of cumulative UV lamp irradiation. Similarly, the afterglow decay behaviours are similar to that of SMT, with small fluctuations in amplitude. After 180 h of cumulative UV irradiation, the attenuation rates of PL intensity in different periods were measured. Figure S8 shows the comparison of attenuation rates of SMT coating, UV-36 h, and UV-180 h SMT coating. In the time periods of 5-10 and 10-20 min, the attenuation rates gradually increase, but the range of fluctuations is small. However, in the following time periods, their afterglow decay rates have changed to different extents. In order to explore the relationship between the doping ratio of powder and polymer. Four groups of coatings containing varying amounts of modified $SrAl_2O_4$: Eu^{2+}, Dy^{3+} powder were placed in a UV lamp (Figure S8). When the doping ration reaches a 40%, the luminescent intensity remained almost constant with the increasing of doping ratio. After cumulative exposure of 180 h, the samples still retained a brightness that was recognizable by the naked eye in darkness (Figure S10). This indicates that the SMT coating maintained its luminescent properties over prolonged UV irradiation, allowing for visibility in low-light or dark conditions. Furthermore, under the ultraviolet lamp, the state and luminance of the SMT coating were recorded through the camera every 36 h (Figure S11). It can be concluded from the observation that there is no significant difference in the luminescence brightness of the coating as the cumulative exposure time of the ultraviolet lamp increases. It is explained that the SMT coating possesses excellent UV weathering resistance, this is attributed to the polyphenol structure with tannic acid in the SMT system[53]. The SMT coating was applied to the wing of the aircraft model (Figure 4c) and the surface of the submarine model (Figure 4d), and then the models were placed under a UV lamp (365nm).

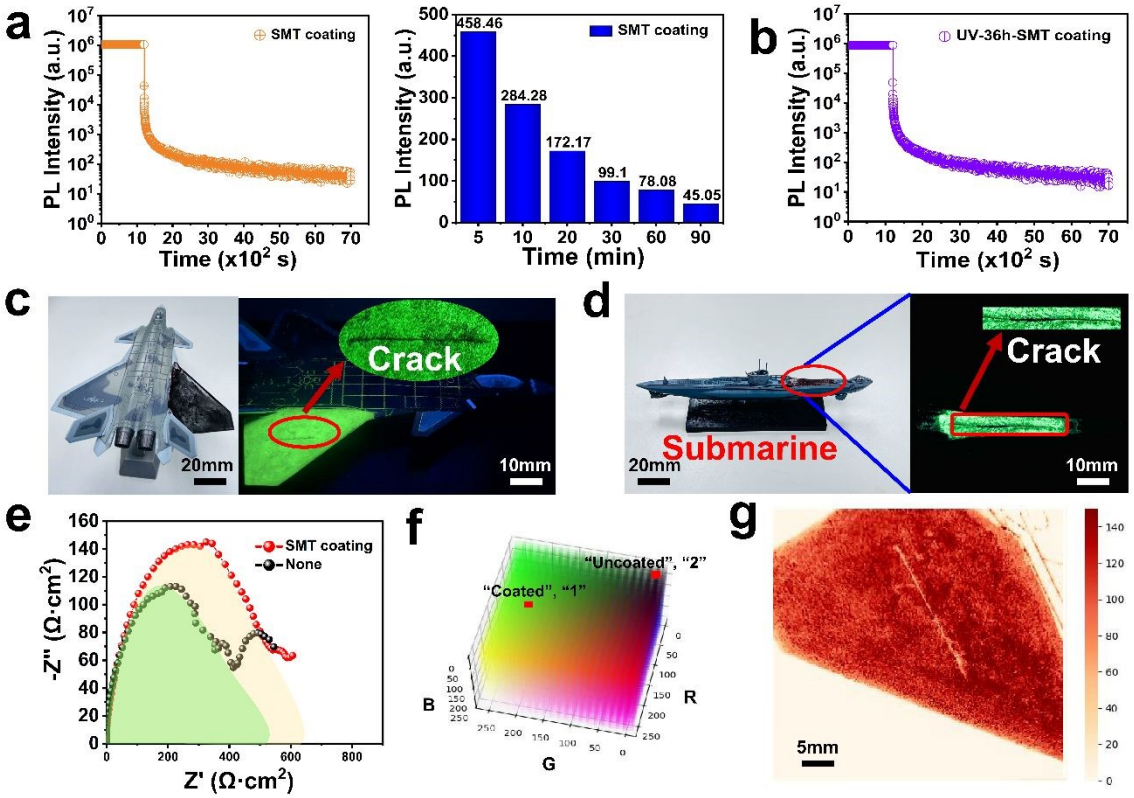

Figure 4. (a) Photoluminescence (PL) intensity with time for SMT coating. (b) PL intensity with time for UV-36 h SMT coating. (c, d) The demonstration images of the SMT coating on the model of an airplane and a submarine alloy model, c is the Chinese J-20 aircraft model; d is submarine alloy model. (e) Nyquist plots of pure carbon steel (none) and SMT coating coated carbon steel electrodes immersed in 3.0 wt.% NaCl solution. (f) 3D CIE RGB chromaticity diagram of SMT coating. (g) Heat map generated based on the green intensity of the aircraft model.

Simultaneously, cracks were artificially induced in the coating using a surgical blade. It can be clearly observed that the brightness of the cracks is significantly weaker than that of other areas. Organic coating on metal substrate is an effective means to delay the corrosion rate of metal substrate by preventing metal substrate from contacting with corrosive medium. EIS measurements were conducted to characterize the anticorrosion performance of the SMT coating coated sheet iron. The measurements were performed under alternating current signal with frequencies from 10^5 to 10^{-1} Hz. Figure 4e shows the EIS results (Nyquist Plot) for SMT coating coated sheet iron. The coatings were coated on sheet iron, and then, the sheet iron was immersed in 3.0 wt.% NaCl. In general, a wider diameter of the semicircle in the Nyquist plot indicates better corrosion resistance, whereas a smaller semicircle diameter and impedance suggest a higher corrosion rate[54]. From the Nyquist plots in Figure 4e, the SMT coating coated

View Article Online
DOI: 10.1039/D4PY00857J

steel has the largest semicircle diameter and impedance value. The impedance of SMT coating coated sheet iron is 145 Ω·cm^2, while that of the pure iron sheet is 113 Ω·cm^2, and its impedance value is increased by 28.31%, indicating it possesses anticorrosion performance.

According to the theory of three primary colors, the luminescence could be quantitatively analyzed by the intensity of three basic colors, red (R), green (G), and blue (B). From the photos of Figure 4c, the RGB values of the luminescent area could be read as 97, 230 and 79, respectively, while the values of the background are 1, 4, 21. Here, according to our developed 3D CIE RGB chromaticity diagram (Figure 4f), it can be easily found out that the intensity of the green color is the key difference in color distributions. By extracting the intensity of green intensity in the image pixel by pixel and constructing a matrix to generate a heat map, as shown in Figure 4g, the distribution of green luminescence can be presented in real-time (Movie S2), which is expected to greatly benefit the identification of crack areas. Moreover, by searching the boundaries of intensity distribution pixel by pixel, the cracks could be presented more intuitively, as shown in the right part, and the theoretical analysis accuracy could approach pixel level (Figure S12).

SMT coating degradation and $SrAl_2O_4$: Eu^{2+}, Dy^{3+} powder recycle

Based on the concept of sustainable development of environmental protection, the biodegradability of this bio-source coating was further studied. Figure 5a shows the degradation of SMT coating in bamboo powder with the increase in burial time. Different colored arrows were used to represent different components, where red circle, blue circle, green circle, black circle, and yellow circle representing SMT coating, bamboo powder, $SrAl_2O_4$: Eu^{2+}, Dy^{3+} powder, coating

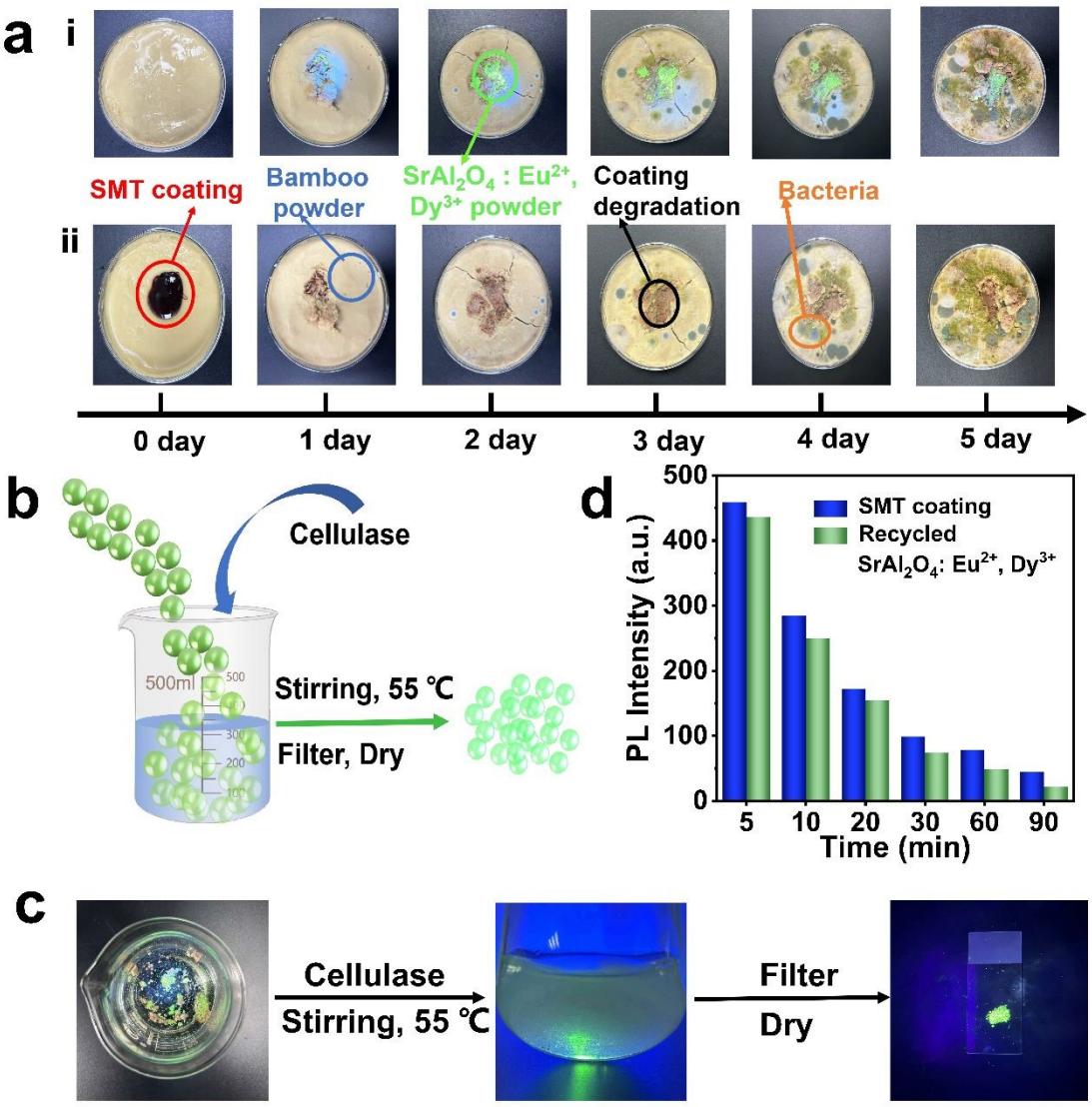

Figure 5. (a) Degradation process of SMT coating buried in bamboo powder. i represents the image of the SMT coating degradation process under ultraviolet flashlight irradiation, and ii represents the image of the SMT coating degradation process under sunlight. Different colored arrows were used to represent different components. (b) Schematic of the $SrAl_2O_4$: Eu^{2+}, Dy^{3+} powder recycle process. (c) The $SrAl_2O_4$: Eu^{2+}, Dy^{3+} Powder recycle process. (d) PL intensity comparison between recycled $SrAl_2O_4$: Eu^{2+}, Dy^{3+} powder and SMT coating. After Xe lamp is used as excitation source and continuously excited for 20 min, PL intensity for different time points is collected.

View Article Online
DOI: 10.1039/D4PY00857J

degradation, and bacteria respectively. SMT coatings can be degraded in bamboo powder, and the degree of degradation increases with the increase of burial days. After 5 days of burial, SMT coating cannot be observed by the naked eye. SMT coating is exposed to open environment (Hainan province, tropical area of China) for six months without degradation. As supplied in Figure S13, after six months there is no visible difference contrast to newly fabricated samples, corresponding FTIR spectra as supplied in Figure S14 also maintain consistent. Finally, colonies were also observed in the degradation chain (Figure S15). The SMT coating could only degraded under anaerobic composting conditions with the help of specific kinds of microorganisms[55, 56]. Figure 5b, c shows the recycling process of degraded powder. The mixture of $SrAl_2O_4$: Eu^{2+}, Dy^{3+} powder and bamboo powder were placed in a container, the further degradation of bamboo powder was achieved by cellulase. The modified $SrAl_2O_4$: Eu^{2+}, Dy^{3+} powder can be recycled. Upon subjecting the recycled powder to FTIR analysis (Figure S16), it is evident that the characteristic peak at 1090 cm^{-1} belongs to the Si-O bond, confirming the retention of the silica layer on the powder's surface. Figure 5d shows the comparison of PL intensity between recycled $SrAl_2O_4$: Eu^{2+}, Dy^{3+} powder and SMT coating at different time points, the intensity of the afterglow decreased little at these six-time points of 5, 10, 20, 30, 60, and 90 min and maintaining the PL intensity of the recycled powder at 95.19% at the time points of 5 min. The attenuation curve of the recycled $SrAl_2O_4$: Eu^{2+}, Dy^{3+} powder was compared with that of the modified $SrAl_2O_4$: Eu^{2+}, Dy^{3+} powder (Figure S17). In the periods of 5-10, 20-30, and 60-90 min after the removal of the excitation source, the attenuation degree of the PL intensity of the recycled $SrAl_2O_4$: Eu^{2+}, Dy^{3+} powder surpassed that of the modified $SrAl_2O_4$: Eu^{2+}, Dy^{3+} powder by 5.36%, 20.72%, and 21.91%, respectively. However, during the periods of 10-20 and 30-60 min, the attenuation rate of the recycled $SrAl_2O_4$: Eu^{2+}, Dy^{3+} powder was found to be lower than that of the modified $SrAl_2O_4$: Eu^{2+}, Dy^{3+} powder, by 2.94% and 13.32%, respectively. It indicates that the luminescence effect of the recycled powder is slightly decreased. Compared with traditional coatings, SMT coatings exhibit remarkable biodegradability, allowing for faster decomposition after disposal, thus significantly reducing pollution to the ecological environment. Furthermore, the recycling and reuse of $SrAl_2O_4$: Eu^{2+}, Dy^{3+} powder comply with the requirements of the circular economy, embodying the green, circular, and low-carbon development philosophy.

Conclusion

An environmental-friendly and bio-degradable intelligent coating based on bio-sourced polymers and modified long afterglow powders was presented. The dynamic hydrogen bonding network endows the coating with desired adhesive performances (313.96 KPa) and self-healing ability (self-healing efficiency 81.29%). By compositing with SiO_2-modified $SrAl_2O_4$: Eu^{2+}, Dy^{3+} powders and developing quantitative luminescence-analysing tool, the intelligent coating with long afterglow ability is able to visualized monitor small cracks. Moreover, the obtained bio-sourced composites could be degraded under anaerobic composting conditions within 5 days, and after degradation the long afterglow powders could be separated and recycled with an almost consistent performances (luminescent intensity maintains 95.19%) contrast to original powders. This work not only provides a valuable example for bio-sourced intelligent coatings, but also open up new opportunities for the utilization of bio-sourced materials.

Conflicts of interest

There are no conflicts to declare.

Data availability

All data included in this study are available upon request by contact with the corresponding author.

Acknowledgements

The authors thank the Innovational Fund for Scientific and Technological Personnel of Hainan Province (KJRC2023C09), Start-up Scientific Research Foundation from Hainan University (KYQD(ZR)22174), Opening Project of Guangxi Key Laboratory of Calcium Carbonate Resources Comprehensive Utilization (HZXYKFKT202301).

References

1. T. Yimyai, D. Crespy and M. Rohwerder, *Advanced Materials*, 2023, **35**, 2300101.
2. D. Zang, R. Zhu, W. Zhang, X. Yu, L. Lin, X. Guo, M. Liu and L. Jiang, *Advanced Functional Materials*, 2017, **27**, 1605446.
3. Y. Ye, Z. Liu, W. Liu, D. Zhang, H. Zhao, L. Wang and X. Li, *Chemical Engineering Journal*, 2018, **348**, 940-951.
4. C. Liu, H. Zhao, P. Hou, B. Qian, X. Wang, C. Guo and L. Wang, *ACS Applied Materials & Interfaces*, 2018, **10**, 36229-36239.
5. C. Zhu, Y. Fu, C. Liu, Y. Liu, L. Hu, J. Liu, I. Bello, H. Li, N. Liu, S. Guo, H. Huang, Y. Lifshitz, S.-T. Lee and Z. Kang, *Advanced Materials*, 2017, **29**, 1701399.
6. B. Zhang, G. Yang, W. Xu, J. Duan and B. Hou, *Journal of Materials Science & Technology*, 2024, **184**, 256-268.
7. Y. Bai, T. Guo, J. Wang, J. Gao, K. Gao and X. Pang, *Acta Materialia*, 2021, **217**, 117179.
8. W. Gu, W. Li, Y. Zhang, Y. Xia, Q. Wang, W. Wang, P. Liu, X. Yu, H. He, C. Liang, Y. Ban, C. Mi, S. Yang, W. Liu, M. Cui, X. Deng, Z. Wang and Y. Zhang, *Nature Communications*, 2023, **14**, 5953.
9. X. Qi, D. Zhang, Z. Ma, W. Cao, Y. Hou, J. Zhu, Y. Gan and M. Yang, *ACS Nano*, 2018, **12**, 1062-1073.
10. J. Liu, F. Recupido, G. C. Lama, M. Oliviero, L. Verdolotti and M. Lavorgna, *Collagen and Leather*, 2023, **5**, 8.
11. S. Gazzotti, M. Hakkarainen, C. A. Pagnacco, M. Manenti, A. Silvani, H. Farina, L. Arnaboldi and M. A. Ortenzi, *Polymer Chemistry*, 2024, **15**, 2081-2093.
12. S. L. Wright and F. J. Kelly, *Environmental Science & Technology*, 2017, **51**, 6634-6647.

13. Y. W. Chek and D. T.-C. Ang, *Progress in Organic Coatings*, 2024, **188**, 108190.
14. Z. Song, F. Gao, W. Zhang, J. Zhong, Y. Wu, Y. Liu, X. Gao and L. Shen, *Progress in Organic Coatings*, 2023, **183**, 107816.
15. P. Feng, H. Wang, S. Gan, B. Liao and L. Niu, *Small*, 2024, **n/a**, 2312085.
16. S. Tang, J. Li, R. Wang, J. Zhang, Y. Lu, G.-H. Hu, Z. Wang and L. Zhang, *SusMat*, 2022, **2**, 2-33.
17. F. Vidal, E. R. van der Marel, R. W. F. Kerr, C. McElroy, N. Schroeder, C. Mitchell, G. Rosetto, T. T. D. Chen, R. M. Bailey, C. Hepburn, C. Redgwell and C. K. Williams, *Nature*, 2024, **626**, 45-57.
18. N. Zhang, C. Gao, L. Meng and X. Tang, *Carbohydrate Polymers*, 2023, **319**, 121224.
19. J. Ho, B. Mudraboyina, C. Spence-Elder, R. Resendes, M. F. Cunningham and P. G. Jessop, *Green Chemistry*, 2018, **20**, 1899-1905.
20. G. Yang, Z. Gong, X. Luo, L. Chen and L. Shuai, *Nature*, 2023, **621**, 511-515.
21. P. Sun, S. Mei, J.-F. Xu and X. Zhang, *Advanced Science*, 2022, **9**, 2203182.
22. C. R. Westerman, B. C. McGill and J. J. Wilker, *Nature*, 2023, **621**, 306-311.
23. X. Fang, N. Tian, W. Hu, Y. Qing, H. Wang, X. Gao, Y. Qin and J. Sun, *Advanced Functional Materials*, 2022, **32**, 2208623.
24. S. Ammar, A. W. M. Iling, K. Ramesh and S. Ramesh, *Progress in Organic Coatings*, 2020, **140**, 105523.
25. X.-Y. Jian, Y. He, Y.-D. Li, M. Wang and J.-B. Zeng, *Chemical Engineering Journal*, 2017, **326**, 875-885.
26. H. Tong, H. Li, H. Li, Cidanpuchi, F. Wang and W. Liu, *Inorganic Chemistry*, 2021, **60**, 15049-15054.
27. X. Chen, G. Wang, M. Wu, J. Liu, Z. Liu, X. Wang, Y. Zou and K. Zhang, *Polymer Chemistry*, 2022, **13**, 4641-4649.
28. Z. Huang, B. Chen, B. Ren, D. Tu, Z. Wang, C. Wang, Y. Zheng, X. Li, D. Wang, Z. Ren, S. Qu, Z. Chen, C. Xu, Y. Fu and D. Peng, *Advanced Science*, 2023, **10**, 2204925.
29. X. Yang, G. I. N. Waterhouse, S. Lu and J. Yu, *Chemical Society Reviews*, 2023, **52**, 8005-8058.
30. S. Liu, N. Mao, Z. Song and Q. Liu, *ACS Applied Materials & Interfaces*, 2022, **14**, 1496-1504.
31. Y. Zhou, P. Zhang, Z. Liu, W. Yan, H. Gao, G. Liang and W. Qin, *Advanced Materials*, 2024, **n/a**, 2312439.
32. J. Liu, G. C. Lama, F. Recupido, C. Santillo, G. Gentile, G. G. Buonocore, L. Verdolotti, X. Zhang and M. Lavorgna, *Composites Science and Technology*, 2023, **236**, 109993.
33. J. Liu, X. Li, X. Yang and X. Zhang, *Advanced Intelligent Systems*, 2021, **3**, 2000183.
34. L. Zhang, D. Wang, L. Xu and A. Zhang, *Polymer Chemistry*, 2021, **12**, 660-669.
35. S. Y. Zheng, J. Zhou, S. Wang, Y.-J. Wang, S. Liu, G. Du, D. Zhang, J. Fu, J. Lin, Z. L. Wu, Q. Zheng and J. Yang, *Advanced Functional Materials*, 2022, **32**, 2205597.
36. Y. Zhuang and R.-J. Xie, *Advanced Materials*, 2021, **33**, 2005925.
37. S. Timilsina, R. Bashnet, S. H. Kim, K. H. Lee and J. S. Kim, *International Journal of Fatigue*, 2017, **101**, 75-79.
38. J. Liu, F. Zhao, Q. Tao, J. Cao, Y. Yu and X. Zhang, *Materials Horizons*, 2019, **6**, 1892-1898.
39. H. Wu, J. Li, W. Zhang, T. Chen, F. Liu and E.-H. Han, *Chemical Engineering Journal*, 2022, **437**, 135405.
40. J. Chen, Z. Wang, B. Yao, Y. Geng, C. Wang, J. Xu, T. Chen, J. Jing and J. Fu, *Advanced Materials*, 2024, **36**, 2401178.
41. J. Cao, C. Zhou, G. Su, X. Zhang, T. Zhou, Z. Zhou and Y. Yang, *Advanced Materials*, 2019, **31**, 1900042.
42. C.-H. Li and J.-L. Zuo, *Advanced Materials*, 2020, **32**, 1903762.
43. Y. Guo, X. An and X. Qian, *ACS Applied Materials & Interfaces*, 2023, **15**, 19362-19373.
44. T. Qi, H. Xia, Z. Zhang, S. Kong, W. Peng, Q. Zhao and Z. Huang, *Solid State Sciences*, 2017, **65**, 88-94.
45. Y. Chen, F. Tian, J. Yao, L. Li, Y. Cui, H. Yang, Z. Chen, G. Sun, P. S. Shuttleworth and H. Yue, *ACS Applied Polymer Materials*, 2024, **6**, 6469-6481.
46. H. Long, L. Hu, F. Yang, Q. Cai, Z. Zhong, S. Zhang, L. Guan, D. Xiao, W. Zheng, W. Zhou, Y. Wei, K. Frank and X. Dong, *Composites Part B: Engineering*, 2022, **239**, 109968.
47. K.-X. Hou, P.-C. Zhao, L. Duan, M. Fan, P. Zheng and C.-H. Li, *Advanced Functional Materials*, 2023, **33**, 2306886.
48. X. Huang, X. Yang, H. Liu, S. Shang, Z. Cai and K. Wu, *Industrial Crops and Products*, 2019, **139**, 111540.
49. X. Wang, X. Huang, Z. Ji, H. Sheng and H. Liu, *ACS Sustainable Chemistry & Engineering*, 2024, **12**, 7147-7157.
50. Y. Ma, Y. Hu, Z. Kou, M. Zhang, L. Hu, S. Li, Q. Huang, P. Jia, Y. Zhou and F. Chu, *Industrial Crops and Products*, 2024, **209**, 118048.
51. Z. Xu, L. Chen, L. Lu, R. Du, W. Ma, Y. Cai, X. An, H. Wu, Q. Luo, Q. Xu, Q. Zhang and X. Jia, *Advanced Functional Materials*, 2021, **31**, 2006432.
52. H. Zhang, B. Wang, J. Han, X. Shen, Q. Sun, Y. An, R. Luo and Y. Wang, *Chemical Engineering Journal*, 2024, **482**, 149020.
53. R. Wang, X. Wang, Y. Zhan, Z. Xu, Z. Xu, X. Feng, S. Li and H. Xu, *ACS Applied Materials & Interfaces*, 2019, **11**, 37502-37512.
54. J. Tong, W. Pan, J. Ma, J. Luo and R. Liu, *Progress in Organic Coatings*, 2023, **175**, 107366.
55. M. S. Kim, H. Chang, L. Zheng, Q. Yan, B. F. Pfleger, J. Klier, K. Nelson, E. L. W. Majumder and G. W. Huber, *Chemical Reviews*, 2023, **123**, 9915-9939.
56. M. Guicherd, M. Ben Khaled, M. Guéroult, J. Nomme, M. Dalibey, F. Grimaud, P. Alvarez, E. Kamionka, S. Gavalda, M. Noël, M. Vuillemin, E. Amillastre, D. Labourdette, G. Cioci, V. Tournier, V. Kitpreechavanich, P. Dubois, I. André, S. Duquesne and A. Marty, *Nature*, 2024, **631**, 884-890.

View Article Online
DOI: 10.1039/D4PY00857J

Data availability

All data included in this study are available upon request by contact with the corresponding author.